WATER RESOURCES RESEARCH, VOL. 36, NO. 2, PAGES 381–393, FEBRUARY 2000

Dripping into subterranean cavities from unsaturated fractures under evaporative conditions

Dani Or and Teamrat A. Ghezzehei

Department of Plants, Soils and Biometeorology, Utah State University, Logan

Abstract. Water dripping into subterranean cavities within fractured porous media is studied in order to improve estimates of dripping rates, drop sizes, and chemical composition of droplets that could affect long-term integrity of waste disposal canisters placed in caverns. Steady state liquid flux in fracture surfaces supported by flow in partially liquid-filled grooves and liquid films in adjacent planes was calculated as a function of the matric potential (vapor pressure) of the fracture. At an intersection of a vertical fracture with a wider cavity the liquid flux feeds a growing pendant drop that eventually detaches. Equilibrium state size and approximate shape of liquid drops suspended from the cavity ceiling were determined from lateral and vertical force balance considering capillarity, gravity, and hydrostatic pressure. A one-dimensional, viscous extension model with appropriate gravitational and surface tension components was employed to determine dripping rate from specified fracture roughness geometry as a function of matric potential (flux). The effect of evaporation from drop surface during drop formation was incorporated; the resulting alterations in drop volume, dripping rate, and drop solute concentration were determined. To facilitate experimental testing of the proposed model, a decoupled solution that considers independently controlled flux and evaporation is presented. Under evaporative conditions, dripping in finite period is possible only when volumetric flux exceeds evaporative demand. Calculations indicate that dripping rate and solute concentration are extremely sensitive to ambient matric potential. The results of this work may be extended to study other phenomena including formation and growth of stalactites and rivulet flow in cave ceilings.

1. Introduction

Drops of water may form in fractured porous media under certain flow and humidity conditions, especially for rock fractures that open into larger subterranean cavities or contain large asperities under unsaturated state [*Ho*, 1997]. Impact of liquid drops on long-term durability of nuclear waste disposal canisters placed in subterranean caverns is an important environmental problem. Dripping characteristics that can be used to study and assess the long-term effect of dripping on canisters may include weight and solute concentration of individual drops and the dripping rate. Additionally, several other phenomena could benefit from improved understanding of dripping, including formation and growth of stalactites and the onset of rivulet flow in fracture walls.

The formation and detachment of drops is a result of motion of free liquid surfaces and the balance between competing forces (e.g., capillary, viscous, gravitational, and inertial). Two extreme conditions that result in drop formation have been a source of wide interest in the past: jetting and slow dripping [*Eggers*, 1997].

When a fluid is ejected at high velocity from a nozzle, a steady jet is formed which subsequently breaks up into small drops due to Rayleigh instability [*Clift et al.*, 1978]. Jetting appears in many engineering problems, including extraction processes, spraying, and ink-jet printing technologies [*Zhang and Basaran*, 1995]. The other extreme condition is drop formation due to very slow release of liquid from a nozzle (dripping). At first, surface-tension forces are in balance with the gravitational force. With slight incremental increases in the drop weight the hanging drop goes through a sequence of equilibrium shapes irrespective of the flow. The static aspects of the sequence depend entirely upon a dimensionless parameter known as the Bond number $Bo = \rho g R^2/\sigma$, where ρ is the liquid density, g is acceleration of gravity, R is the drop radius, and σ is the surface tension of the liquid [*Eggers*, 1997]. At a later stage, gravity overcomes the surface tension, and the drop begins to fall and eventually detaches. The period of evolution leading to detachment is determined by another dimensionless parameter, the Reynolds number $Re = R\sigma/\rho\eta^2$, which includes the dependence on the liquid viscosity (η) [*Eggers*, 1997].

A complete description of evolution of drop size and shape as well as the detachment period requires use of the three-dimensional Navier-Stokes equations with free boundary conditions. Such analyses are inherently complicated and obviate derivation of analytical solutions. Numerical simulations require high computational resolution, long computation time with results limited to the special conditions studied [*Eggers and Dupont*, 1994]. There have been attempts by several authors to simplify the system into a one-dimensional (axisymmetrical) problem that ignores the details of drop shape evolution yet retains the nonlinear physical behavior and mathematical tractability. A useful one-dimensional axisymmetric solution that applies for flow regimes of intermediate velocity, compared to the jetting and dripping processes discussed above, has been proposed by *Wilson* [1988]. Wilson's

Paper number 1999WR900311.
0043-1397/00/1999WR900311$09.00

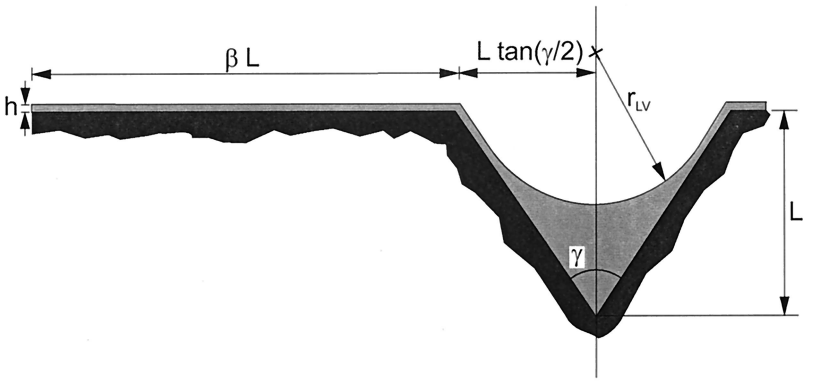

Figure 1. Definition sketch of a unit fracture surface-roughness element in a horizontal cross section. A groove is defined by its depth (L) and angle (γ). The attached plane for film flow is proportional to the groove depth with coefficient β.

analysis involves the balance between viscosity, gravity, and surface tension during the drop growth and detachment stages, while ignoring the effect of inertia.

The formation of droplets in cavities raises the vapor pressures on the drop surface to above saturation [*Ho*, 1997] inducing evaporation from the drop surface. The vapor pressure gradient between the drop surface and the ambient environment is intensified when the vapor pressure in the cavities is below saturation. Hence the significance of evaporation is especially important at low dripping rates and/or low vapor pressures of the ambient atmosphere. Assuming isothermal diffusion rate governed by Fick's law, *Ho* [1997] presents a simple solution to the evaporation rate from a spherical drop of a fixed radius.

D. Or and M. Tuller (Flow in unsaturated porous media–Hydraulic conductivity of rough fracture surfaces, submitted to *Water Resources Research*, 1999) (hereinafter referred to as Or and Tuller, submitted manuscript, 1999) present an alternative modeling approach for flow on unsaturated rough fracture surfaces, considering flow regimes in thin films and corners (or grooves). The special geometrical features of the model allow the direct calculation of liquid fluxes along vertical fractures of fixed cross-sectional geometry, as a function of the ambient vapor pressure (matric potential). When the fractures open into cavities, low liquid flux in the fractures may result in the formation of droplets, whose detachment rate is governed primarily by the flux and hence the equilibrium vapor pressure.

The objective of this study was to develop an integrated model for drop formation at the intersection of a vertical unsaturated fracture with an open cavity, large enough to accommodate maximum drop size, considering effects of evaporation. We present an adaptation of *Wilson*'s [1988] one-dimensional solution for dripping rate from the lip of an unsaturated rough fracture into a cavity. For situations where the vapor pressure in the fractures is in equilibrium with that in the cavity, drop growth and simultaneous evaporation from drop surfaces are coupled by the matric potential. For non-equilibrium scenarios (e.g., actively ventilated cavity), drop formation and evaporation are controlled by different vapor pressures in the fractures and the cavity. The solution to the latter scenario is specifically useful for testing the model experimentally, with independently controlled flux and relative humidity of the cavity.

2. Theoretical Considerations

The theoretical section is organized as follows: Characterization of liquid flow in a unit fracture element is presented in section 2.1. Transition in liquid energy state and configuration of drops at the intersection of fractures with cavities is discussed briefly in section 2.2 with details given in appendix A. Adaptation of a one-dimensional dripping model [*Wilson*, 1988] to the fracture model is considered in section 2.3. The effect of steady state evaporation from the drop surface is incorporated into previous derivations in section 2.4. The upper limit of dripping period due to the competing effects of low flux and high evaporation under low potentials is presented in section 2.5. Methods of calculating the drop volume under evaporative and nonevaporative conditions are presented in section 2.6. Finally, the effect of different potentials on the solute concentration of liquid drops is presented in section 2.7.

2.1. Flow on Rough Fracture Surfaces

Or and Tuller (submitted manuscript, 1999) have developed a new model for flow on rough surfaces of unsaturated rock fractures. We present here only derivations related to the calculation of liquid flux contributing to drop formation. The model considers a unit cross-sectional segment of a fracture with wide aperture and consists of flow regimes in thin films and in partially filled grooves (corner flow). For the purposes of this study we will use a surface roughness element with cross-sectional view as depicted in Figure 1 comprising a vertical groove and adjacent plane surface. Water flow occurs in thin films over the plane surface element of width (βL) and in the groove defined by the depth (L) and angle (γ).

A curved liquid-vapor interface in equilibrium with the matric potential at ambient atmosphere (ψ) is maintained in the groove. The interface curvature follows the Young-Laplace relationships until a geometry-dependent critical matric potential (ψ_c) is reached, above which the groove is completely liquid-filled,

$$\psi_c = \frac{\sigma}{L}\frac{\cos(\gamma/2)}{\tan(\gamma/2)}. \quad (1)$$

The radius of curvature of the liquid-vapor interface (r_{LV}) in the groove, prior to fill-up by liquid, is given by the Young-Laplace equation,

$$r_{LV} = -\frac{\sigma}{\psi}. \quad (2)$$

The film thickness (h) over the plane area is related to the matric potential by [*Iwamatsu and Horii*, 1996]

$$h = \sqrt[3]{\frac{A_{SVL}}{6\pi\psi}}, \quad (3)$$

where A_{SVL} is the Hammaker constant, a thermodynamic adsorption parameter for solid-vapor interactions through the intervening adsorbed liquid.

The flux of liquid flow ($m^3\ s^{-1}$) across the cross-sectional area of the element (Figure 1) is calculated for unit gravitational gradient. The individual contributions of film and groove flow to the total flux prior and after groove fill-up are given in subsections 2.1.1 and 2.1.2.

2.1.1. Partially saturated pits/grooves ($\psi < \psi c$). Expressions for film flow are derived from standard Navier-Stokes equations with appropriate boundary conditions and from consideration of changes in the contributing cross-sectional area of the film with changes in the matric potential. The volumetric film flux Q_F is given by

$$Q_F = \frac{h^3\rho g}{3\eta}\left\{\beta L + 2\left[\frac{L}{\cos(\gamma/2)} - \frac{r_{LV}}{\tan(\gamma/2)}\right]\right\}. \quad (4a)$$

Expressions for average liquid velocity in corners/grooves bounded by a liquid-vapor interface were derived by *Ransohoff and Radke* [1987], and the volumetric corner flux Q_C is

$$Q_C = \frac{r_{LV}^4 F\rho g}{\varepsilon\eta}, \quad (4b)$$

where ε is a dimensionless flow resistance parameter dependent on groove angle (γ) according to $\varepsilon = \exp(2.214 + 0.00783\ \gamma)$, for $10° < \gamma < 150°$ [*Ransohoff and Radke*, 1987], and F is a dimensionless angularity factor, defined by groove geometry,

$$F = \frac{1}{\tan(\gamma/2)} - \pi\frac{180 - \gamma}{360}. \quad (5)$$

2.1.2. Completely filled pits/grooves ($\psi > \psi_c$, close to saturation). Similarly, for near-saturation state (completely filled grooves), equivalent expressions for volumetric fluxes of film flow (Q_F) and corner flow (Q_C) were derived as

$$Q_F = \frac{h^3\rho g}{3\eta}[\beta L + 2L\tan(\gamma/2)] \quad (6a)$$

$$Q_C = L^2\tan(\gamma/2)\frac{r_{LV}^2\rho g}{\varepsilon\eta}. \quad (6b)$$

The total flux, $Q = Q_F + Q_C$, due to film and groove flow feeds a pendant drop formed at the bottom tip of the groove. Note that both film thickness (h) and radius of capillary curvature (r_{LV}) are functions of the matric potential (ψ).

2.2. Liquid Behavior at Dripping Plane

The intersection of a vertical, wide fracture surface with a subterranean cavity results in an abrupt change in energy state of the groove liquid. For slow fluxes and wettable rock (contact angle between liquid-vapor interface and solid $\theta < 90°$) the liquid reaching the bottom of the groove accumulates and forms a pendant drop. Figure 2a depicts formation of pendant water drop at the bottom tip of a vertical groove constructed on an aluminum slab ($L = 3.5$ mm and $\gamma = 60°$). The effect of the liquid pressure in the drop (as determined by the size and shape of the drop) propagates back to form a transitional zone of liquid configuration different from that up in the groove. For subsequent analysis of drop formation and detachment we require a boundary condition in the form of solid-liquid interface area (Ao) that anchors a pendant drop to the cavity ceiling. In section A1 we present a simplified geometrical model for the determination of approximate shape and size of pendant drops by accounting for the major force components. The results of the calculations in section A1 and experimental observations (an example is shown in Figure 3) indicate that the drop anchoring area (Ao) is only weakly dependent upon groove geometry and drop size, with a narrow range of calculated drop diameter (9.8–11.8 mm). These results are consistent with the observations of *Curl* [1972] regarding the existence of a minimum diameter of stalactites of (5.1 mm) that are presumably formed within drop boundaries and thus imply minimum drop diameter. Constant drop anchoring areas (Ao) that can be used in subsequent section are listed in Table 1. The drop shape and size were also used to derive simple analytical expressions for the transitional, groove-liquid profile above the dripping plane in section A2.

2.3. One-Dimensional Axisymmetric Dripping Model [*Wilson*, 1988]

We consider liquid emerging from the bottom of a groove at a very slow flow velocity that does not induce jetting ($Re < 1$). The liquid forms a drop that grows slowly and stretches under its own weight until it raptures and detaches. During drop growth a force balance between viscosity, gravity, and surface tension determines its evolution. The effect of inertia on drop formation and detachment is neglected. For simplicity, we start by presenting the evolution of the first drop from the emergence of the first liquid element at the groove tip to its detachment. Later, the periodicity and evolution of all subsequent drops are considered.

At the base of a fracture, liquid leaves the groove at a volumetric flux Q, forming an axisymmetrical drop with constant, liquid-solid interface area (Ao). To track the growth and detachment of the drop, we switch to a Lagrangian coordinate system, as shown in Figure (2b). The fluid elements are labeled by their time of emergence (τ) from the groove bottom, and the actual time is denoted by (t). The first element to leave the groove is labeled by $\tau = 0$, and the element just leaving at present time is labeled as $\tau = t$, and $0 \le \tau \le t$ on all other points. Let $X_{t,\tau}$ be the distance bellow the groove bottom of a typical element labeled by τ, at time t, and let $A_{t,\tau}$ be the cross-sectional area of the drop corresponding to that element. Considering two neighboring elements τ and $\tau + d\tau$, the conservation of volume (assuming the liquid is incompressible) leads to

$$Q\ d\tau = -A_{t,\tau}\ dX_{t,\tau}. \quad (7)$$

First, consider a drop forming in the absence of the effect of surface tension. We employ force balance between the two neighboring elements τ and $\tau + d\tau$, where the longitudinal stress on the horizontal section is denoted by $S_{t,\tau}$. Then,

$$(SA)_\tau - (SA)_{\tau+\Delta\tau} = \rho g A_{t,\tau}\ dX_{t,\tau} = \rho g Q\ d\tau. \quad (8)$$

Thus

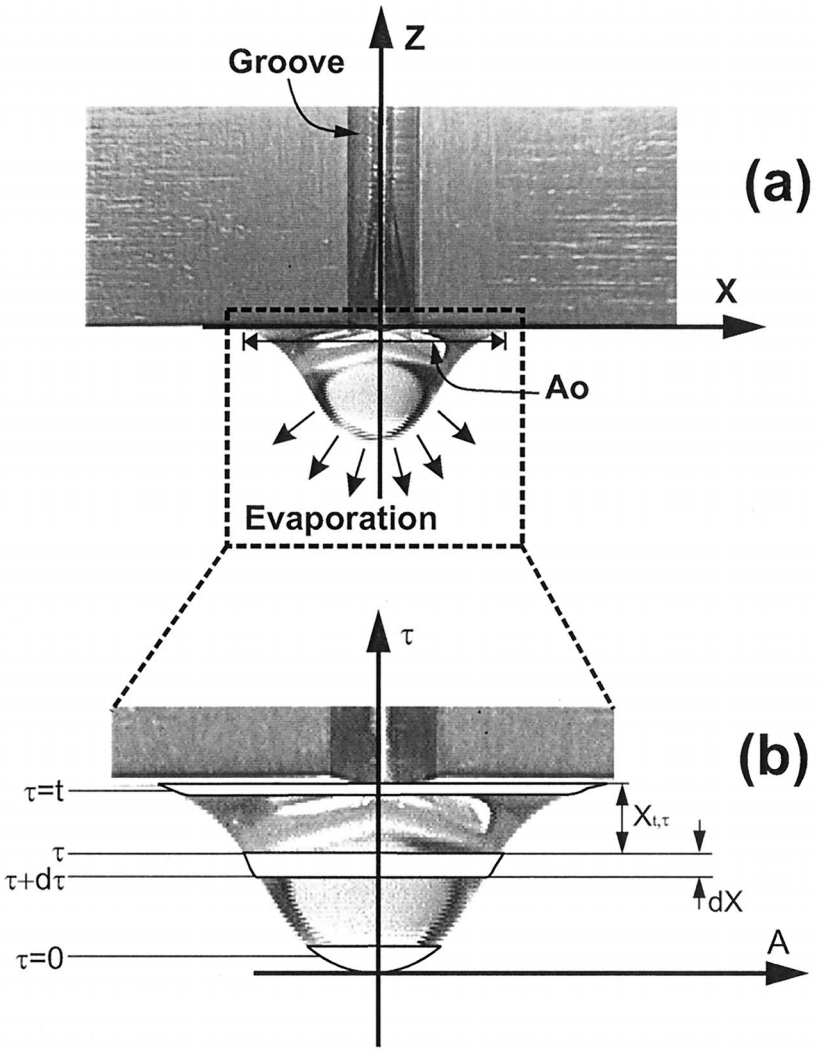

Figure 2. Definition diagram showing a drop forming into a cavity from the face of a fracture roughness model (aluminum slab with vertical grooves): (a) Cartesian coordinate system and (b) Lagrangian coordinate system. Elements of the drop in horizontal plane are marked by a moving (in time).

$$\frac{\partial}{\partial \tau}(SA) = \rho g A \frac{\partial X}{\partial \tau} = \rho g Q. \tag{9}$$

Then, (9) can be integrated to give

$$(SA)_{t,\tau} = \rho g V_{t,\tau}, \tag{10}$$

where the drop volume is defined as $V_{t,\tau} = Q\tau$. Qualitatively, (10) states that the longitudinal force at any element marked by τ equals the weight of the fluid underneath it.

Table 1. Calculated Drop Anchoring Radius (R) for Two Groove Angles (γ) and Two Contact Angles (θ)

	R, mm			
	$\gamma = 30°$		$\gamma = 120°$	
λ	$\theta = 0°$	$\theta = 30°$	$\theta = 0°$	$\theta = 30°$
1	5.73	4.99	5.73	4.89
1.1	5.74	5.02	5.75	4.95
1.2	5.76	5.03	5.76	4.97
1.3	5.77	5.05	5.77	5.01
1.4	5.79	5.07	5.71	4.95
1.5	5.80	5.27	5.70	5.19

The effect of liquid surface tension acting against gravity can be introduced into (10). The surface tension of the liquid acts along the perimeter ($p_{t,\tau}$) of the drop,

$$S_{t,\tau} = \left(\frac{\rho g Q\tau - p\sigma}{A}\right)_{t,\tau}, \tag{11}$$

where $S_{t,\tau}$ is vertical stress acting in a horizontal cross section of drop at an element defined by τ, $p_{t,\tau}$ is the perimeter of drop cross section at element τ, and $A_{t,\tau}$ is the liquid cross section of a drop at element τ.

The rate of extension of the drop is related to the stress by the constitutive equation of elongational flow assuming a Newtonian flow:

$$S = -3\eta \frac{1}{A}\frac{\partial A}{\partial t} - \frac{1}{2}\frac{p}{A}\sigma, \tag{12}$$

where η is the viscosity of water. The second term on the right-hand side of (12) is a correction accounting for resistance to extension of the cross-sectional area due to surface tension. As the drop begins to detach, the cross-sectional area in the necking area (A) shrinks (takes opposite sign). Hence the

stress due to viscous deformation (first term on the right-hand side of (12)) opposes the surface tension, having an effect of added drop weight. The apparent influence of this phenomenon on the drop volume will be discussed in section 3.2.

Equations (11) and (12) are combined to give the following, first-order differential equation:

$$\frac{\partial A(t)}{\partial t} = \frac{-\rho g Q \tau + \pi \sigma R(t)}{3\eta}. \tag{13}$$

Equation (13) can be integrated to give

$$A(t) = \frac{(UQ\tau)^2}{W} \cdot \left\{ 1 + \text{product log}\left[\frac{-\exp\left(-1 + \frac{W(t-C)}{6\eta UQ\tau} \right)}{UQ\tau} \right] \right\}^2, \tag{14}$$

where $U = \rho g$, $W = \pi\sigma^2$, and C is the constant of integration determined using the boundary condition $A = \text{Ao}$ at $t = \tau$. The special function product log $(z) = \omega$ is the solution to the nonlinear expression $z = \omega e^{\omega}$ [*Abramowitz and Stegun*, 1974]. Ao is the solid-liquid interface area at the dropping plane given in Table 1;

$$C = \frac{\tau}{W}\left\{ W - 6\eta UQ - 6\eta UQ \cdot \ln\left[-\exp\left(-1 + \frac{\sqrt{\text{Ao}W}}{UQ\tau} \right) \sqrt{\text{Ao}W} - UQ\tau \right] \right\}. \tag{15}$$

The drop is pinched and detaches in a finite time (t) where the drop cross sectional area $A(t)$ goes to zero. The time at which this occurs is obtained by setting (14) to zero,

$$t = \tau - 6\eta \sqrt{\frac{\text{Ao}}{W}} \left[1 + \frac{Q\tau}{\Omega} \ln\left(1 - \frac{\Omega}{Q\tau} \right) \right], \tag{16}$$

where $\Omega = \sqrt{\text{Ao}W}/U$.

The drop element (plane) that vanishes first also satisfies an additional condition: $dt/d\tau = 0$. This leads to an implicit solution for the critical fluid element of breakage or detachment τ_c from (16),

$$1 - 6\eta \sqrt{\frac{\text{Ao}}{W}} \left[\frac{1}{Q\tau_c - \Omega} + \frac{1}{\Omega} \ln\left(1 - \frac{\Omega}{Q\tau_c} \right) \right] Q = 0. \tag{17}$$

Values of τ_c for different matric potentials and geometries are obtained by an iterative (numerical) solution of (17). Comments on the solution methods used are provided in appendix B. The time at which the first drop detaches is obtained by substituting τ_c into (16). The drop volume (V_d) is obtained simply by integrating the volumetric flux over the duration of drop formation (from $\tau = 0$ to $\tau = \tau_c$):

$$V_d = \tau_c Q. \tag{18}$$

At the time of detachment of the first drop (t_c^1) a portion of the extruded liquid at the tip of the groove remains suspended. The volume of the remaining liquid (also known as the recoil volume) is associated with the time difference $(\tau_0 = t_c^1 - \tau_c)$. Because all subsequent drops are built on existing recoil volume, the period of detachment after the first drop pinches is reduced by the time equivalent to the recoil volume (τ_0),

$$t_c = t_c^1 - \tau_0 = \tau_c \tag{19}$$

In other words, (19) states that the volume of liquid extruded from the outlet during an interval between two successive drops is equal to the drop volume.

2.4. Evaporation From Drop Surface

For the relatively slow rates of unsaturated surface flows in fractured porous media, evaporation from drop surface can greatly increase the time required for drop detachment, especially under drier conditions. Low matric potentials induce reduction in influx (Q) and extend detachment period (τ_c) thereby increasing the opportunity time for evaporation. At the same time, evaporative demand by the surrounding atmosphere increases with reduced vapor pressure. A diffusion type equation of radial evaporation [*Ho*, 1997] is used to incorporate the competing effects of evaporation on drop growth and detachment period.

For mathematical simplicity we assume a hemispherical drop shape during its formation time. The time sequence photographs of a drop growing and detaching under a constant flux shown in Figure 3 indicate that the drop shape is approximately hemispherical for more than 4/5 of the entire period (denoted as drop formation period). Significant deviation from hemispherical shape occurs only for a short period before detachment (detachment period). The rapid detachment period is less sensitive to variation in flux than the formation period. *Zhang and Basaran* [1995] have shown that the detachment period of drops released from a pipe of fixed radius remains approximately constant as flux decreases, while the drop formation period (with hemispherical drop shape) increases by a few orders of magnitude. This further justifies the hemispherical assumption, because evaporation starts to affect drop formation and detachment significantly only when the flux is very low.

The instantaneous rate of evaporation from a droplet of radius (r_b) can be assumed to be isothermal diffusion process as represented by Fick's law [*Ho*, 1997],

$$\frac{dr_b}{dt} = -\frac{D}{\rho}\frac{dC}{dr}\bigg|_{r=r_b}, \tag{20}$$

where dr_b/dt is rate of change in the drop radius (m s^{-1}), D is binary diffusion coefficient of water vapor (m^2 s^{-1}), and dC/dr is the water vapor concentration gradient (kg m^{-3} m^{-1}).

The binary diffusion coefficient of water vapor (D) at ambient temperature (T) is related to binary diffusion coefficient (D°) at standard temperature and pressure by [*Campbell*, 1986]

$$D = D^{\circ}\frac{10^5}{P}\left(\frac{T}{273.15} \right)^{1.8}, \tag{21}$$

where P is the total gas pressure (1.0×10^5 Pa at sea level). The concentration gradient of water vapor at the drop surface is obtained by solving for radial diffusion from the drop surface [*Ho*, 1997],

$$\frac{dC}{dr}\bigg|_{r=r_b} = \frac{\Delta P_v}{r_b R^* T}, \tag{22}$$

where R^* is the water vapor gas constant ($R^* = 462$ J kg^{-1} K^{-1}) and ΔP_v is the difference in vapor pressure between the drop surface and the surrounding environment. This pressure

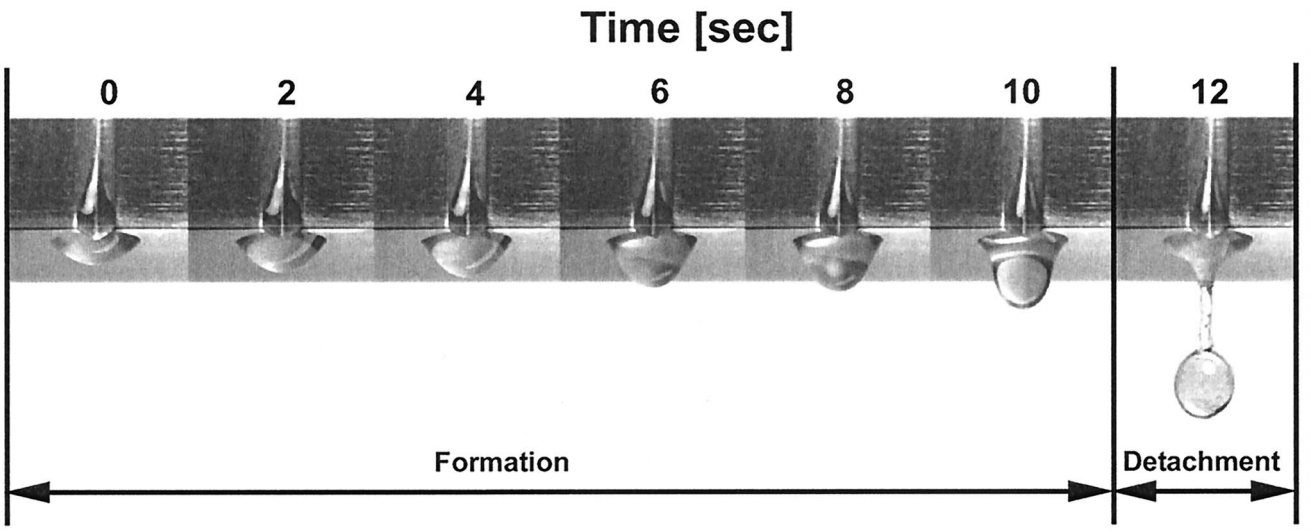

Figure 3. Time sequence photographs of water drop formation and detachment from vertical grooves (L = 3.5 mm, $\gamma = 60°$, and $Q \cong 1$ cm^3 min^{-1}). Note that the drop anchoring area (Ao) does not change. The drop has approximately hemispherical shape for the first 5/6 time of the total formation period (drop formation period); in the remaining 1/6 of the period the drop forms a neck and detaches (drop detachment period).

difference is related to the matric potential (ψ) and the saturated vapor pressure of ambient temperature (P_{sat}) by

$$\Delta P_v = P_{\text{sat}}\left[1 - \exp\left(\frac{\psi\rho}{R^*T}\right)\right]. \tag{23}$$

The initial radius (r_{b0}) for a hemispherical drop in the absence of evaporation is related to the flux by

$$r_{b0}(\tau) = \sqrt[3]{\frac{3Q}{2\pi}\tau}. \tag{24}$$

Integration of (20) with the initial condition given by (24) leads to an expression for the instantaneous drop radius:

$$r_b^2(\tau) = \frac{2D\Delta P_v}{\rho R^*T} + r_{b0}(\tau)^2. \tag{25}$$

The corresponding drop volume considering evaporation would be

$$V(\tau) = \frac{2\pi}{3} r_b(\tau)^3 = \frac{2\pi}{3}\left[\frac{2D\Delta P_v}{\rho R^*T}\tau + \left(\frac{3Q}{2\pi}\tau\right)^{2/3}\right]^{3/2}. \tag{26}$$

The net flux at any given element (τ) is obtained by differentiating (26):

$$Q_{\text{net}}(\tau) = \frac{2\pi}{3\tau}(M\tau + N\tau^{2/3})^{3/2}, \tag{27}$$

where $M = -(2D\Delta P_v)/(\rho R^*T)$ and $N = (3Q/2\pi)^{2/3}$.

In the presence of evaporation the flux (Q) in (14) is replaced by Q_{net} in (27). After some algebraic manipulations, as shown in the case of nonevaporative conditions, we arrive at a similar expression for time to detachment,

$$t = \tau - 6\eta\sqrt{\frac{\text{Ao}}{W}}\left[1 + \frac{Q_{\text{net}}(\tau)\tau}{\Omega}\ln\left(1 - \frac{\Omega}{Q_{\text{net}}(\tau)\tau}\right)\right]. \tag{28}$$

The first drop element to reach a pinching state satisfying the additional condition $dt/d\tau = 0$ is derived from (28):

$$1 - 6\eta\sqrt{\frac{\text{Ao}}{W}}\left[\frac{1}{Q_{\text{net}}(\tau_c)\tau_c - \Omega} + \frac{1}{\Omega}\ln\left(1 - \frac{\Omega}{Q_{\text{net}}(\tau_c)\tau_c}\right)\right]Y = 0, \tag{29}$$

with $Y = (d/d\tau)[Q_{\text{net}}(\tau_c)\tau_c] = \pi/3\ (N\tau_c^{2/3} + M\tau_c)^{1/2}(2N\tau_c^{-1/3} + 3M)$.

Equation (29) is evaluated by an iterative procedure. Comments on the special features of (29) and solution methods adopted in this study are provided in appendix B.

2.5. Maximum Detachment Time

For liquid drops to be formed and eventually detach, the net liquid flux feeding them must be positive at all stages. If, at any stage of drop formation, the net flux becomes negative, the drop would decrease in size (because of higher evaporation rate than influx) and never attain sufficient weight to break off. For any given matric potential (vapor pressure) the time (τ) which equates the term on the right-hand side of (27) to zero represents the maximum opportunity time ($\tau_{\max}$) within which the drops would be formed and detach:

$$\tau_{\max} = \left(\frac{R^*T\rho}{2D\Delta P_v}\right)^3\left(\frac{3Q}{2\pi}\right)^2. \tag{30}$$

Drop detachment time (τ_c) is obtained as a solution to (29) and must be less than the maximum opportunity time ($\tau_{\max}$). For negative net flux (Q_{net}), (29) is mathematically undefined.

2.6. Drop Volume

The volume of the individual drops is obtained by integrating the net flux (27) over the duration of the drop formation (from $\tau = 0$ to $\tau = \tau_c$):

$$V_d = 4\pi\,[(-8N^4\sqrt{N\tau_c^{2/3}} + (N + M\tau_c^{1/3})^2 V_d \cdot (8N^2 - 20MN\tau_c^{1/3} + 35M^2\tau_c^{2/3})\sqrt{N\tau_c^{2/3} + M\tau_c}) \cdot (315M^3\tau_c^{1/3})^{-1}]. \tag{31}$$

The total volume of water that leaves the groove is given by integrating the constant influx over the duration of drop formation

$$V_t = Q\tau_c. \tag{32}$$

The difference between the total influx (V_t) and the drop volume (V_d) represents the volume of water that evaporates during drop formation.

2.7. Solute Concentration in Drops

During drop formation, water preferentially evaporates leaving behind nonvolatile solutes (salts) thereby changing the solute concentration of the growing drop. The ratio of the total liquid volume entering the drop to the detached drop volume can be interpreted as the relative increase in solute concentration of the drop at the time of detachment:

$$C_{\text{rel}} = \frac{C_{\text{drop}}}{C_0} = \frac{V_t}{V_d}, \tag{33}$$

where C_{drop} and C_0 are the concentrations of the drop liquid and bulk liquid feeding the drop, respectively. Dryer conditions induce slow flow rates and longer detachment times, as well as higher evaporative demand. When these processes are coupled, they result in high solute concentrations in drops formed under low matric potentials (dry conditions). The effect of increased solute potential on evaporation rates, potential gradients, and solute diffusion are not considered in this analysis and require further investigation.

3. Illustrative Examples

Illustrative calculations of drop detachment period, drop volume, and relative concentration at detachment are presented in Figure 4. The groove depth used for the calculation was $L = 2$ mm deep, equivalent to typical surface roughness observed by *Tokunaga and Wan* [1997] and the associated plane width of ($\beta = 1$). Comparisons between two groove angles (30° and 120°) are presented. In the following examples, matric potential is measured in units of energy per unit volume [J m^{-3}] (1 J m^{-3} = 1 Pa = 10^{-3} J kg^{-1} = 0.1 mm H_2O). In these examples we consider a water flux induced by a unit gravitational gradient. However, the mathematical solutions can accommodate fluxes due to gradients other than unity (e.g., nonvertical fractures) or externally imposed fluxes. It is assumed that the matric potentials in the fracture and the cavity are at equilibrium.

3.1. Detachment Time

As discussed in section 2.2 and in Appendix A, the drop shape and anchoring area are not significantly affected by the groove geometry. However, groove geometry significantly affects the dripping by varying the flux (Q) associated with any given matric potential (ψ). Of the three geometric parameters (L, β, and γ) that define the fracture surface roughness, the groove angle (γ) results in the largest variations in dripping rates. A narrow groove angle can support larger cross-sectional area of capillary water hence higher liquid flux at any given matric potential. The effect of groove depth (L) is limited to determining the matric potential of complete filling of the grooves. The parameter β does not have significant effect on dripping rate and drop size since corner flow dominates film flow by several orders of magnitude in the range of matric potential where drop formation is possible (near saturation).

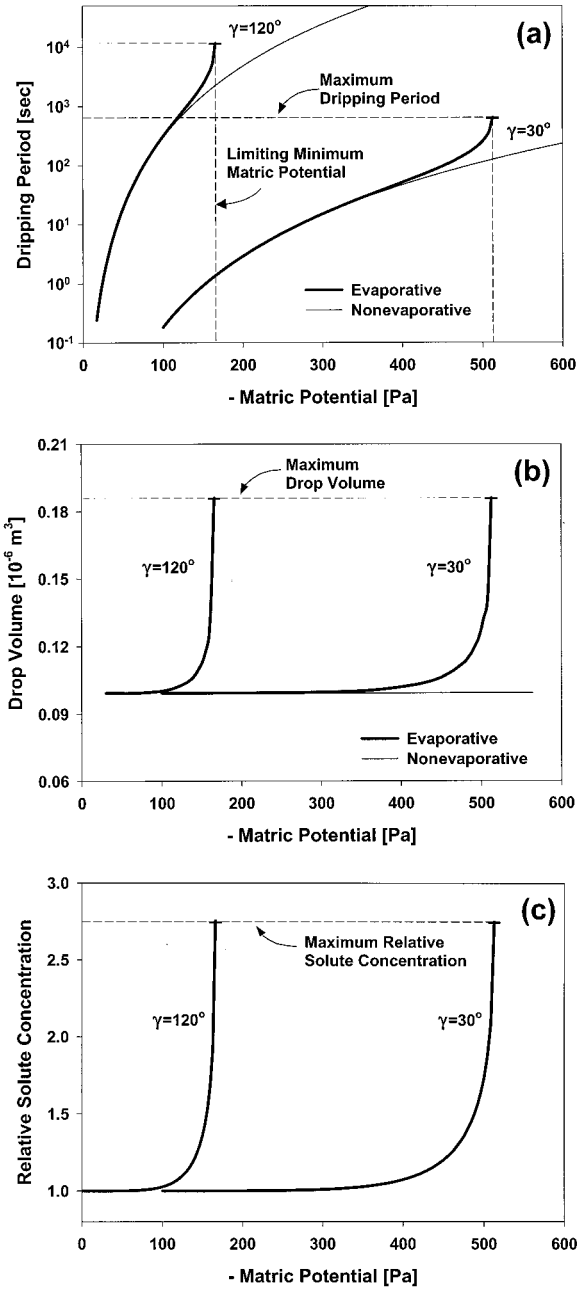

Figure 4. Theoretical dripping characteristics dependent on coupled matric potentials (ψ) of cavities and fractures. (a) Drop detachment time (τ_c) under evaporative and nonevaporative conditions. (b) Drop volume at detachment under evaporative and nonevaporative conditions. (c) Relative solute concentration of drops at detachment time.

The detachment periods (τ_c) for evaporating and nonevaporating conditions for two groove angles are depicted in Figure 4a. As the matric potential decreases (becomes more negative), the total influx (Q) decreases, resulting in longer dripping period of individual liquid drops. When we consider the evaporative condition, as matric potential decreases, the competition between the decreasing influx and increasing evaporation rate results in a significant rise in dripping period

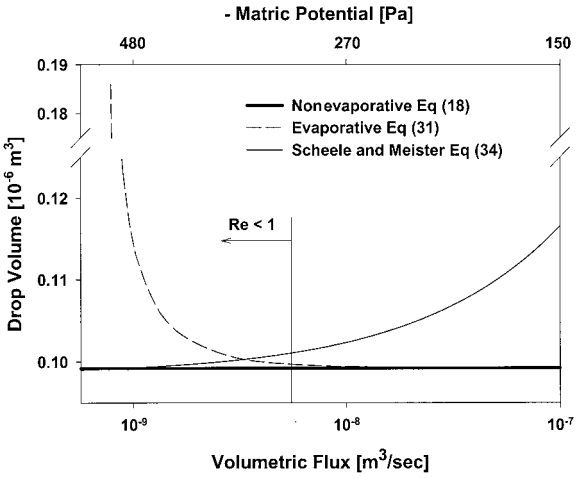

Figure 5. Comparison of drop volume under nonevaporative (equation (18)) and evaporative conditions (equation (31)) with a semiempirical equation of *Scheele and Meister* [1968] (equation (34)).

until a limiting minimum matric potential is reached. At ambient condition drier than the limiting minimum matric potential, there would not be enough flux to exceed the evaporative demand, and dripping ceases. In contrast, under nonevaporating conditions (equation (17)), drop formation continues indefinitely with no bounds on minimum matric potential. At any given matric potential, because narrow groove angles (γ) result in higher flux (while evaporative demand is independent of the groove geometry), they have lower, limiting-minimum matric potential.

3.2. Drop Volume

The volume of individual drops as a function of the matric potential is shown in Figure 4b. The drop volume is primarily determined by the drop anchoring area (Ao) and time to detachment (τ_c). The drop anchoring area does not change with groove geometry and matric potential; hence there is no significant change in drop size (volume) associated with the drop anchoring area (Ao).

The dependence of drop volume on the duration of drop formation is through the rate of viscous extension (equation (12)). Under evaporative conditions the net flux (equation (27)) decreases during the growth period of individual drop, reaching a minimum just before detachment ($\tau = \tau_c$). As the ambient matric potential approaches the limiting-minimum matric potential (indicated by the vertical marker in Figure 4a), the minimum net flux (Q_{net}) approaches zero because of increased evaporative demand. Hence the downward stress component due to viscous extension decreases as the drop grows (see discussion in section 2.3). The increased upward stress component allows additional drop weight to be suspended as indicated by the rapid rise in drop volume in Figure 4b. The maximum drop volume corresponds to the maximum equilibrium drop weight that can be suspended in the absence of viscous energy dissipation and hence is independent of flux as shown in Figure 4b.

3.3. Solute Concentration

Solute concentration of individual drops is directly related to the volume of the evaporated water (difference between the total influx and the net flux). Solute concentration of drops at time of detachment ($\tau = \tau_c$) are shown in Figure 4c for two groove angles (γ) as functions of the matric potential (ψ). The effect of lower matric potential on drop solute concentration is through the decrease in dripping rate that allows more evaporation to take place. At potentials close to limiting minimum matric potential, the time required for drop formation increases rapidly thereby allowing for extended evaporation opportunity times. Near this region (see Figure 4a for the fast rise in formation time) the concentration more than doubles by only a slight decrease in potential (or vapor pressure). It is important to note that the limiting minimum potential (below which dripping stops) is completely determined by the groove angle (γ). This sensitivity to groove angle and matric potential variations guarantees that even under similar ventilation conditions, variations in individual dripping rates among grooves of different groove angles would produce drops with different solute concentrations. In general, slow pathways would result in higher relative solute concentration of drops by allowing longer evaporation duration. Similarly, even slight variations in matric potential (e.g., at a range that could be induced even by barometric pressure or temperature variations) near the minimum drop-forming matric potential could substantially alter solute concentration of drops. There are nominal changes that do not take into consideration the effect of deposition such as observed in Karst system where P_{CO_2} is lower in the cavity [*White*, 1988].

3.4. Comparison With Alternative Solution of Scheele-Meister

We compared our drop volume calculations with a widely used semiempirical equation of *Scheele and Meister* [1968]. The original equation was developed based on a two-stage process of formation of a liquid drop (growing and necking) into a different liquid. For liquid drop forming in air, the Scheele-Meister equation can be reduced to [*Zhang and Basaran*, 1995]

$$V_{\text{SM}} = F_{\text{HB}}\left[\frac{2\pi\sigma\text{Ro}}{g\rho} - \frac{4Q^2}{3\pi\text{Ro}^2 g} + 7.14\left(\frac{Q^2\text{Ro}^2\sigma}{g^2\rho}\right)^{1/3}\right] \quad (34)$$

where Ro is the radius of inlet area, and F_{HB} is the Harkins-Brown correction factor to account for the fraction of an ideal pendant (static) drop that detaches. Comparisons between our drop volume calculations and those of the Scheele-Meister equation (Figure 5) were done using the Harkins-Brown factor as the fitting parameter ($F = 0.5$). The Scheele-Meister equation was formulated to account for inertial effects on drop volume, whereas the Wilson model of slow dripping does not consider inertia [*Zhang and Basaran*, 1995]. Hence the comparisons are valid only for low Reynolds number ($Re < 1$), where the match is excellent. When $Re = 15$, the Scheele-Meister equation yields drop volume higher than our calculations by 15%. Finally, because the Scheele-Meister equation was not formulated to account for evaporation, the comparison under evaporative conditions is not applicable.

4. Alternate Solution for Experimental Purposes

Tests of the fracture-dripping model presented in this paper require an experimental setup in which accurately controlled flux and vapor pressure induce dripping. Such an experiment could be designed around accurate control of vapor pressure in the experimental fracture and cavity. However, the fact that liquid flux and evaporation are inseparable presents a formi-

dable challenge to practical experimental systems. To alleviate the above shortcomings, we present a decoupled solution in which the liquid influx and evaporation are controlled independently. This approach can also be used in investigating real-life problems where drop formation under equilibrium state vapor pressure is not possible (e.g., actively vented cavities).

We consider a setup consisting of a sample of fractured media similar to Figure 2, in which the plane width parameter is set as $\beta = 0$ (considering flow in grooves only). A controlled steady state volumetric flux is applied at the groove top (Q_V). This influx of liquid substitutes the chemical-potential-dependent flux (Q) of previous calculations.

The applied flux is not permitted to overflow out of the grooves (by keeping the flux sufficiently small or using deep grooves). Thus the flow mechanism is similar to that of corner flow in partially filled grooves given in (4b).

The net flux (Q_{net}) given in (27) is modified by substituting Q with Q_V. The drop detachment time is obtained by solving (29) using the modified net flux and similar methods discussed in section 2.3. The evaporation from drop surfaces is determined by the matric potential in the cavity (ψ_{cav}). Sample calculations of drop detachment times (τ_c) for a series of fluxes (Q_V) and different cavity matric potentials (ψ_{cav}) are shown in Figure 6a. For a given condition of cavity matric potential (ψ_{cav}) the net flux decreases with decrease in flux, leading to increase in detachment time. When the flux approaches a critical minimum, the competition between influx and evaporation is intensified leading to rapid rise in dripping period and finally termination of dripping. The minimum volumetric fluxes (Q_{min}) and maximum dripping periods associated with a wide range of ambient vapor pressures of fracture cavity are depicted in Figure 6b. When the vapor pressure of the cavity is close to saturation (e.g., $\psi = -1$ Pa), the effect of evaporation is negligible and drops can be formed from very small volumetric fluxes in a very long dripping period. More ventilated cavities (lower cavity matric potential, ψ_{cav}), however, require higher minimum-volumetric flux to generate dripping and, consequently, have a lower maximum dripping period.

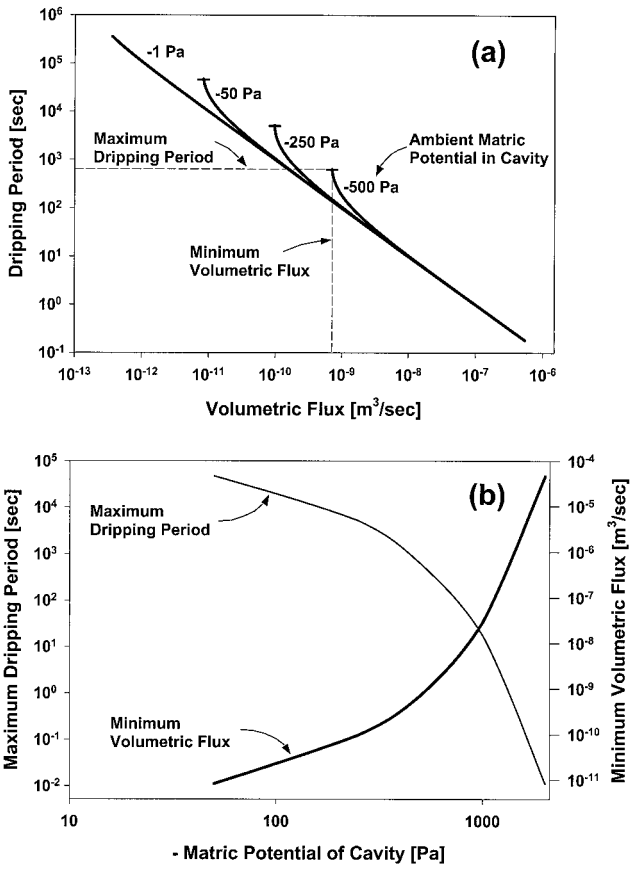

Figure 6. Theoretical dripping characteristics determined by decoupled (independent) liquid flux and evaporative conditions (matric potential of cavity) for a groove angle $\gamma = 30°$. (a) Dripping period under different cavity ventilation conditions (matric potentials) dependent on volumetric flux. (b) Minimum volumetric flux required to generate dripping under different ventilation conditions (matric potential of cavity) and the associated maximum dripping period.

5. Summary and Conclusions

This work focuses on investigation of the environmental and physical conditions resulting in dripping and provides tools that can be used to study various dripping characteristics occurring under several combinations of fracture geometry and cave ventilation. A mechanistic model for drop formation and detachment from a lip of a vertical fracture intersecting an open cavity was developed. The model is based on combining three elements: (1) unsaturated flow on rough fracture surfaces (Or and Tuller, submitted manuscript, 1999), (2) mechanisms for drop formation and detachment under slow dripping conditions [*Wilson*, 1988], and (3) effects of evaporation from suspended drops [*Ho*, 1997]. Simplifications were introduced into the coupled solution to permit verification of the model for experimentally controlled flux in grooves of known geometry.

The primary results and conclusions of this study are as follows: (1) Spontaneous dripping under natural conditions is sensitive to the ambient water vapor pressure in open cavities and is likely to occur only under very high vapor pressures close to saturation. (2) The model provides predictions of dripping rates, drop sizes, and solute concentrations for a wide range of matric potentials and surface roughness of elements. (3) Rough and highly angular fracture surfaces (small groove angles) are conducive for dripping and expand the range of vapor pressures where dripping is possible. Grooves that are more angular yield faster dripping rates (shorter detachment times) at a given matric potential. (4) The competing effect of evaporation renders drop size, dripping rates (detachment times), and chemical composition of drops very sensitive to minute changes in ambient conditions. (5) Considering variations in natural surface roughness geometry, we expect the combined effects of evaporation and flow rates to induce large variability in dripping rates and drop chemistry even at very small spatial scales (e.g., dripping from the same fracture). (6) The restriction of the calculated drop anchoring area in a narrow range is in qualitative agreement with experimental observations of stalactite [*Curl*, 1972]. This work can be extended to accommodate deposition of calcite due to the combined effects of evaporation from drop surface and existence of P_{CO_2} gradient within a pendant drop [*White*, 1988].

The possibility of feedback mechanisms between evaporation-induced variations in chemical composition of the suspended drop and concurrent changes in evaporation rates and

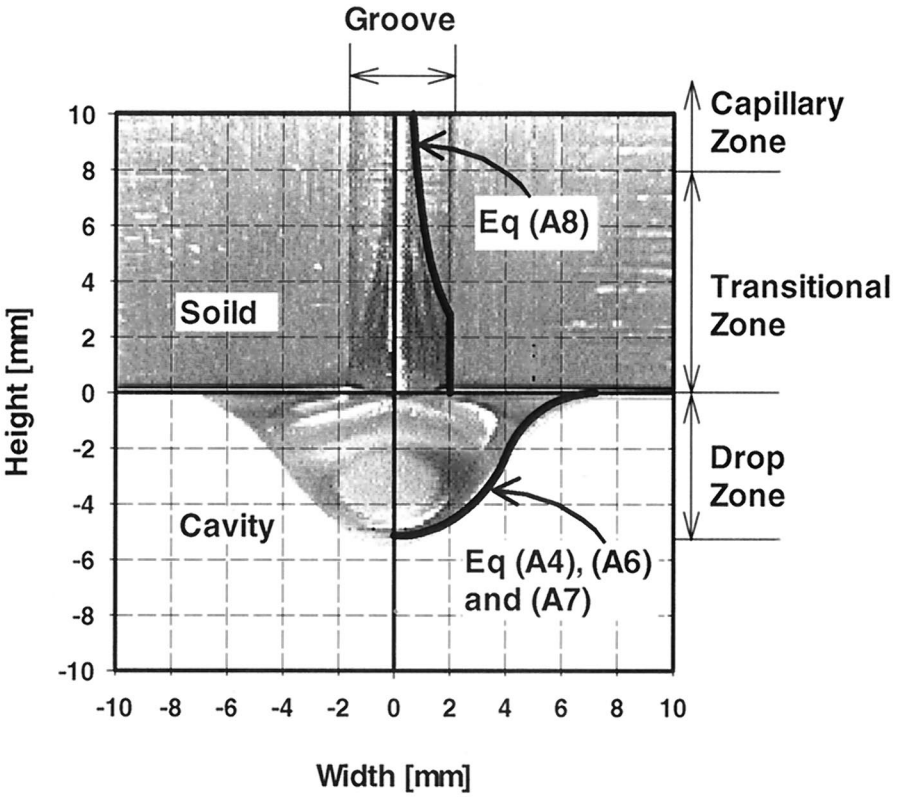

Figure A1. Classification of the dripping flow regime into capillary, transitional, and drop zones. Solid outlines are theoretical profiles of transitional and drop profiles calculated according to simplified methods discussed in appendix A (fixed variables are $L = 3.5$ mm, $\gamma = 60°$, $\theta = 0°$, $\lambda = 1.3$; solved variables are $\phi = 0.02$, $\alpha = 0.75$, $a = 4.5$ mm, and $R = 5.7$ mm).

liquid surface tension properties will be investigated in future studies. Work is underway to study dripping behavior from inclined cavity ceilings where drops are formed and then potentially migrate a certain distance before their detachment. This aspect is particularly important for assessing long-term impact of dripping on waste disposal canisters placed in drifts of different geometry.

Appendix A: Energy Transition and Liquid Profile Near Dripping Plane

The flow domain in vertical grooves dripping into a wide cavity can be classified into three distinct zones, as demarcated in Figure A1. The outlines in Figure A1 correspond to drop and transitional profiles calculated using methods discussed in this appendix.

In the uniform groove-flow zone, the liquid profile and flux are entirely controlled by the matric potential (vapor pressure) of the ambient rock-fracture environment, with few boundary effects emanating from dripping plane. The profile of a pendant drop zone is a result of interaction between capillary forces, surface tension, and gravity. The transitional region provides the necessary pressure adjustment between the pendant drop (superatmospheric) and the capillary liquid of the grooves (subatmospheric) with gravitational pressure gradient. The primary focus of this appendix is to present a simplified approach for calculating the liquid profiles in (1) the pendant-drop zone and (2) the transitional zone which allows for the determination of the drop anchoring area (Ao). Detailed derivations and comparisons that consider a wide range of conditions will be reported in future work.

A1. Liquid Profile in the Pendant Drop Region

Equilibrium-state shape and size of pendant liquid drops is primarily governed by the balance between gravity, surface tension, and pressure [*Boucher and Evans*, 1975, 1980]. The pressure difference across the liquid-vapor interface of a pendant drop suspended from a solid ceiling (Figure A1) at any vertical plane below the supporting ceiling is given by the Young-Laplace equation,

$$\Delta p(z) = \sigma\left(\frac{1}{R1(z)} + \frac{1}{R2(z)}\right), \tag{A1}$$

where z is vertical distance from the supporting ceiling, $\Delta p(z)$ is pressure difference across the drop surface at z ($\Delta p(z)$ will be denoted by $p(z)$ hereafter), and $R1(z)$ and $R2(z)$ are principal radii of curvature at z. The pressure gradient along the vertical axis of symmetry is given by

$$\frac{dp(z)}{dz} = -\rho g. \tag{A2}$$

An implicit expression for the drop profile is obtained by integrating (A2) and equating it to (A1):

$$\sigma\left(\frac{1}{R1(z)} + \frac{1}{R2(z)}\right) = -\rho g z + \tilde{p}, \tag{A3}$$

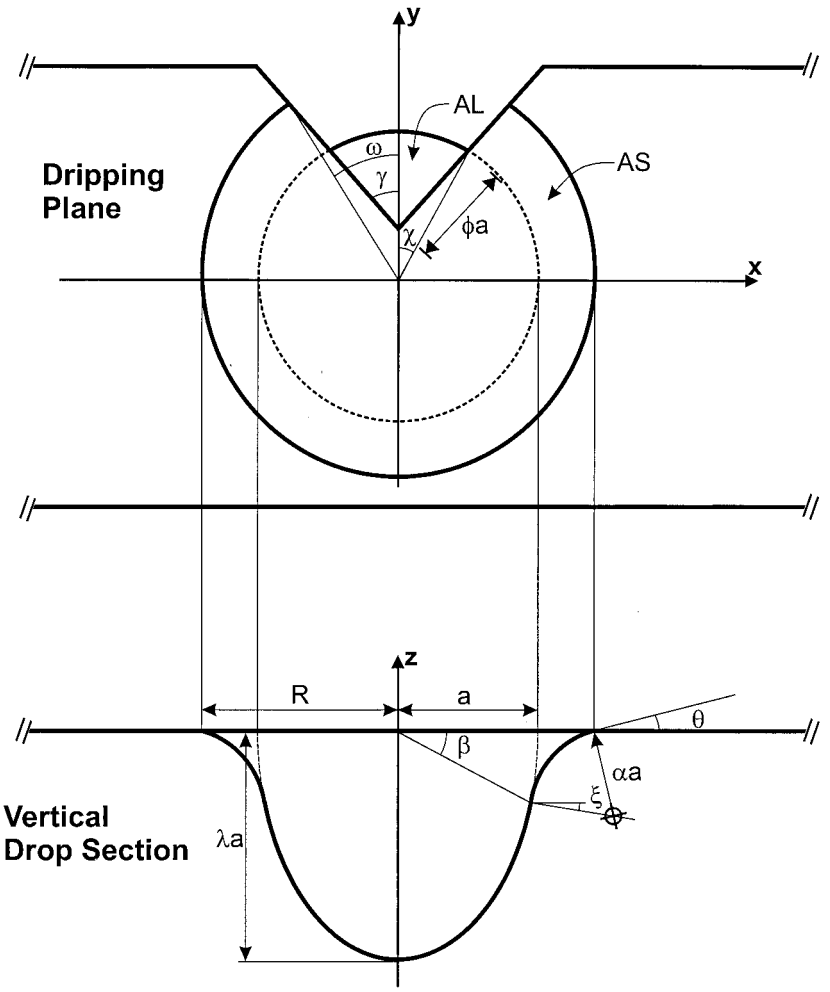

Figure A2. Schematic diagram of the simplified drop model used to calculate drop anchoring area and drop profile.

where $\tilde{p} = 2\sigma/\mathrm{ro}$ is positive pressure at the bottom tip of the drop due to the positive and uniform radius of curvature ro ($R1 = R2 = \mathrm{ro}$) at the bottom tip of the drop.

Closed-form solution for (A3) is not available. Even standard methods of numerical integration suffer from a singularity at the bottom boundary (drop tip). However, liquid drop profiles have been calculated by introducing simplifying expressions and choosing some arbitrary parameters that directly [*Pitts*, 1973] or indirectly fix the drop volume [*Freud and Harkins*, 1929; *Nemchinsky*, 1994].

Both of the above approaches for determination of liquid drop profile provide satisfactory tools based on first principles. However, because of the complicated computational effort involved and complexity stemming from introduction of the effect of grooved inlet, we opted for a simpler geometrical shape that captures most of the physical principles involved.

We define the profile of pendant drop by a semiellipsoid [*Erbil and Meric*, 1997] with the radius in the dripping plane given by a, and λ is the aspect ratio, as shown in Figure A2. The negative liquid pressure beneath the dripping plane required to anchor the drop is created by an arc, with negative curvature of αa, tangential to the ellipsoid and approaching the supporting ceiling at an angle θ (solid-liquid-vapor contact angle). The actual radius of the drop anchoring area is denoted by R. Other geometrical dimensions of the proposed drop shape required to calculate various areas and pressures are defined in Figure (A2).

We consider vertical force balance equations at the cavity ceiling or dripping plane. At $z = 0$ the liquid pressure and surface tension are in balance with the weight of the drop suspended beneath,

$$\bar{P}(\mathrm{AS} + \mathrm{AS}) + 2(\pi - \omega)R \sin(\theta) = V\rho g, \qquad \text{(A4)}$$

where, AS and AL are portions of the drop anchoring area in contact with the solid (cavity ceiling) and groove liquid, respectively. The first term on the left-hand side is force due to mean liquid pressure ($\bar{P}$) acting over the liquid anchoring area (AS plus AL). The second term on the left-hand side corresponds to the upward component of the surface tension acting along the solid-liquid-vapor contact line (perimeter of drop cross section). The right-hand side denotes the weight of the pendent drop. The area-averaged mean liquid pressure is given by

$$\bar{P} = \left[\sigma\left(\frac{1}{R} - \frac{1}{\alpha a}\right)\mathrm{AS} + \frac{2\sigma}{a}\,\mathrm{AL}\right]/(\mathrm{AS} + \mathrm{AL}). \qquad \text{(A5)}$$

An additional constraint requires that the vertical pressure gradient given in (A2) be satisfied. This may be stated as

follows: The difference in capillary pressure between the top and the bottom of the drop is due to the difference in gravitational potential energy,

$$\bar{P} - \frac{2\sigma}{ro} = -\rho g(\lambda a), \tag{A6}$$

where ro is the positive and uniform radius at the drop tip ($ro = \lambda a$).

The horizontal position of the pendant drop in relation to the groove is defined by the relative wetted length of the groove face (ϕ) in Figure A2. Lateral force balance in the direction of the axis of symmetry of the groove (passing through the apex) provides the necessary conditions to determine the horizontal location of the drop. The forces acting in the horizontal direction are due to capillary pressure and surface tension along the solid-liquid-vapor contact line. The positive pressure in the liquid-liquid contact area and negative pressure in the solid-liquid contact area tend to pull the drop toward the groove (outward). While surface tension, acting along the solid-liquid-vapor contact line, pulls the drop away from the groove (inward);

$$\frac{2\sigma}{a} \sin(\chi) - \sigma\left(\frac{1}{R} - \frac{1}{\alpha a}\right) \sin(\bar{\omega}) = 2\bar{\omega}R\sigma. \tag{A7}$$

The drop shape that satisfies the above three balance equations and constraints for fixed contact angle (θ) and aspect ratio (λ) is obtained by solving (A4), (A6), and (A7) simultaneously for a, α, and ϕ. Superposition of calculated drop profile over drop image, shown in Figure A1, indicates good agreement (values of the variables used/solved are given in the caption).

The primary result of these calculations is the drop anchoring area ($Ao \cong \pi R^2$) that provides the boundary condition necessary for solving the one-dimensional axisymmetric dripping model. The drop base area obtained in this fashion has been found to be weakly dependent on the groove angle (γ) but significantly dependent on the contact angle (θ) as shown in Table 1. It has also been shown that the drop radius varies slightly with the drop aspect ratio (λ) or varies indirectly with drop volume. The results indicate that the value of drop anchoring radius (R) has a narrow range (4.9–5.9 mm), and the radius of the ellipsoid (a) is approximately 85% of R. Experimental observations of pendant drops suspended from a grooved aluminum slab further assert the stability of drop anchoring radius (Figure 3). This is also supported by observations of *Curl* [1972] on the existence of a minimum radius of stalactites (2.6 mm), which also implies the existence of minimum drop anchoring area. Consequently, we used drop base area (Ao) that corresponds to the mean drop volume ($\lambda = 1.5$) to approximate a constant boundary condition for the drop detachment model (section 2.3).

A2. Liquid Profile in the Groove's Transitional Zone

The pressure profile in the transition region is determined by integrating (A2) with the initial condition given by the pressure in the liquid-liquid cross section of the drop (AL),

$$P(z) = \frac{2\sigma}{a} - \rho g z, \tag{A8}$$

where $P(z) \geq \psi$. Upper in the groove (in the capillary zone), where $P(z)$ is less than the ambient matric potential ($P(z) < \psi$), the liquid configuration in the grooves is in equilibrium with the ambient matric potential. The calculated liquid profile, obtained from the pressure profile by using (2), shows good agreement with the observed liquid profile in the transitional region (Figure A1).

Appendix B: Numerical Solution of Dripping Period

The equations describing the drop detachment period under nonevaporative (17) and evaporative (29) conditions can be written in general form as

$$1 - 6\eta\sqrt{\frac{Ao}{W}}\left[\frac{1}{Q\tau_c - \Omega} + \frac{1}{\Omega}\ln\left(1 - \frac{\Omega}{Q\tau_c}\right)\right]\frac{\partial}{\partial\tau}(Q\tau) = 0. \tag{B1}$$

The difference between the nonevaporative and evaporative conditions lies in the dependence of the flux (Q) on the drop growth stage (τ). For nonevaporative conditions the entire influx reaching the groove tip contributes to drop formation and is independent of the stage of drop growth hence $\partial(Q\tau)/\partial\tau = Q$. For evaporative conditions, however, the net flux (Q_{net}) is dependent on the drop growth stage (because of the dependence of evaporation rate on drop radius), and $\partial(Q\tau)/\partial\tau$ has a more complicated form.

The left-hand side of (B1) has real values only for $Q\tau > \Omega$ (for positive argument of the logarithm). The function has a very steep slope in a narrow range near the solution ($\tau = \tau_c$) and a very flat slope when $\tau > \tau_c$. Both of these features make standard methods of solving implicit equations (e.g., Newton-Raphson iteration) inapplicable. The numerical scheme used in this paper seeks the solution only in the region of real values by the method of bisection, starting at the point of singularity ($\tau = \Omega/Q$).

Notation

A, Ao, AS, AL	horizontal cross-sectional areas of pendant drop [m].
A_{svl}	Hamaker constant [-6.0×10^{-19} J].
C	water vapor concentration [kg m^{-3}].
C_{rel}, C_{drop}, C_o	solute concentration [kg m^{-3}].
D	binary diffusion coefficient of water vapor in air [m^2 s^{-1}].
D^o	binary diffusion coefficient of water vapor in standard temperature and pressure [2.13×10^{-5} m^2 s^{-1}].
F	angularity factor.
F_{HB}	Harkins-Brown drop volume correction factor ($F_{HB} = 0.48$ in this study).
g	acceleration of gravity [9.81 m s^{-1}].
h	film thickness [m].
L	groove depth [m].
p	perimeter of drop in horizontal cross section [m].
P	total gas pressure [10^5 Pa].
$\bar{P}$	average hydrostatic pressure inside drop [Pa].
P_{CO_2}	partial pressure of CO_2.
P_{sat}	saturated vapor pressure [2337 Pa].
Q, Q_C, Q_F, Q_{net}, Q_v, Q_{min}	volumetric liquid flux [m^3 s^{-1}].
R, Ro	radius of drop in horizontal plane [m].
R^*	water vapor gas constant [462 J kg^{-1} K^{-1}].

r_b radius of assumed hemispherical liquid drops [m].
r_{LV} radius of liquid-vapor interface curvature [m].
S vertical stress acting over horizontal cross section of drop [Pa].
T absolute temperature [293 K].
V_d, V_{SM}, Y_t volume of drop, drop according to *Scheele and Meister* [1968] [ ], total, respectively [m^3].
t actual time [s].
t,τ value of variable (A, p, Q, S, V, and X) for element τ at time t (subscript).
β dimensionless parameter relating plane area to groove depth.
γ groove angle [deg].
ε dimensionless flow resistance parameter.
η liquid viscosity [Pa s].
ρ liquid density [998 kg m^{-3}].
σ surface tension at the liquid-vapor interface [0.0729 N m^{-1}].
τ emergence time for a plane in a Lagrangian coordinate system [s].
τ_c time to detachment [s].
ψ matric potential [J m^{-3}].
ψ_c critical matric potential separating partially filled and full pits [J m^{-3}].

Acknowledgments. The authors express their gratitude to Markus Tuller (USU) for assistance in obtaining time sequence photographs in Figure 3. The authors gratefully acknowledge the partial support of NSF under grant EAR-9805409, the Nuclear Regulatory Commission (NRC) under contract NRC-02-97-009 to the Center for Nuclear Waste Regulatory Analysis (CNWRA), and the Utah Agricultural Experimental Station (UAES). Special thanks to Randal Fedors (CNWRA) and three anonymous reviewers for their thorough review of the manuscript and to Ron Green and Debra Hughson (CNWRA) for many insightful comments. This paper is an independent product of a contract to the CNWRA and does not necessarily reflect the view or regulatory position of the NRC. This is approved as UAES journal paper 7228.

References

Abramowitz, M., and I. A. Stegun, *Handbook of Mathematical Functions, With Formulas, Graphs, and Mathematical Tables*, Dover, Mineola, New York, 1974.

Boucher, E. A., and M. J. B. Evans, Pendant drop profiles and related capillary phenomena, *Proc. R. Soc. London*, *Ser. A*, *346*, 349–374, 1975.

Boucher, E. A., and M. J. B. Evans, XII properties of fluid bridges between solids in a gravitational field, *J. Colloid Interface Sci*., *75*, 407–418, 1980.

Campbell, G. S., *An Introduction to Environmental Biophysics*, Springer-Verlag, New York, 1986.

Clift, R., J. R. Grace, and M. E. Weber, *Bubbles, Drops and Particles*, Academic, San Diego, Calif., 1978.

Curl, R. L., Minimum diameter stalactites, *Bull. Natl. Speleol. Soc*., *34*(4), 129–136, 1972.

Eggers, J., Non linear dynamics and breakup of free-surface flows, *Rev. Mod. Phys*., *69*(3), 865–929, 1997.

Eggers, J., and T. F. Dupont, Drop formation in a one-dimensional approximation of the Navier-Stokes equation, *J. Fluid Mech*., *262*, 205–221, 1994.

Erbil, Y. H., and R. A. Meric, Evaporation of sessile drops on polymer surfaces: Ellipsoidal cap geometry, *J. Phys. Chem. B*, *101*, 6867–6873, 1997.

Freud, B. B., and W. D. Harkins, The shapes of drops, and determination of surface tension, *J. Phys. Chem*., *33*, 1217–1234, 1929.

Ho, C. K., Evaporation of pendant water droplets in fractures, *Water Resour. Res*., *33*(12), 2665–2671, 1997.

Iwamatsu, M., and K. Horii, Capillary condensation and adhesion of two wetter surfaces, *J. Colloid Interface Sci*., *182*, 400–406, 1996.

Nemchinsky, V. A., Size and shape of the liquid droplet at the molten tip of an arc electrode, *J. Phys. D Appl. Phys*., *27*, 1422–1442, 1994.

Pitts, E., The stability of pendent liquid drops, 2, Axial symmetry, *J. Fluid Mech*., *63*, 487–508, 1973.

Ransohoff, T. C., and C. J. Radke, Snap-off of gas bubbles in smoothly constricted noncircular capillaries, *AIChE J*., *33*, 753–765, 1987.

Scheele, G. F., and B. J. Meister, Drop formation at low velocities in liquid-liquid systems, *AIChE J*., *14*, 9–15, 1968.

Tokunaga, T. K., and J. Wan, Water film flow along fracture surfaces of porous rock, *Water Resour. Res*., *33*(6), 1287–1295, 1997.

White, W. B., *Geomorphology and Hydrology of Karst Terrains*, Oxford Univ. Press, New York, 1988.

Wilson, S. D. R., The slow dripping of viscous fluid, *J. Fluid. Mech*., *190*, 561–570, 1988.

Zhang, X., and O. A. Basaran, An experimental study of dynamics of drop formation, *Phys. Fluids*, *7*(6), 1184–1203, 1995.

T. A. Ghezzehei and D. Or, Department of Plants, Soils and Biometeorology, Utah State University, Logan, UT 84322-4820. (Teamrat@mendel.usu.edu; dani@tal.agsci.usu.edu)

(Received March 23, 1999; revised September 14, 1999; accepted October 21, 1999.)